Lin, K.-C., Postdoctoral Research Fellow, The University of Michigan, Ann Arbor, MI.

Sunderland, P.B., Postdoctoral Research Fellow, The University of Michigan, Ann Arbor, MI.

Xu, F., Graduate Student Research Assistant (GSRA) and Postdoctoral Research Fellow, The University of Michigan, Ann Arbor, MI.

---

[a]For the period 1 June 1997-31 May 2000.

D/cw/IN/25

2. Laminar Premixed and Diffusion Flames (Ground-Based Study)

2.1 Introduction

Ground-based studies of soot processes in laminar flames proceeded in two phases, considering laminar premixed flames and laminar diffusion flames, in turn. The test arrangement for laminar premixed flames involved round flat flame burners directed vertically upward at atmospheric pressure. The test arrangement for laminar jet diffusion flames involved a round fuel port directed vertically upward with various hydrocarbon fuels burning at atmospheric pressure in air. In both cases, coflow was used to prevent flame oscillations and measurements were limited to the flame axes. The measurements were sufficient to resolve soot nucleation, growth and oxidation rates, as well as the properties of the environment needed to evaluate mechanisms of these processes. The experimental methods used were also designed to maintain capabilities for experimental methods used in corresponding space-based experiments. This section of the report will be limited to consideration of flame structure for both premixed and diffusion flames, whereas the next section will consider soot growth, nucleation and oxidation properties. The present discussion of the research is brief, more details can be found in Xu et al. (1997,1998,2000a,2000b), Xu and Faeth (2000,2001) and El-Leathy et al. (2001).

Activities carried out in the ground-based study of flame structure are described in the following, considering experimental methods, computational methods, experimental and computational results, and conclusions, in turn.

2.2 Experimental Methods

Premixed Flame Apparatus. Two kinds of premixed burners operating at atmospheric pressure were used for the premixed flame measurements: a 60 mm diameter water-cooled

porous plate laminar premixed flame burner (McKenna Products, Inc.) directed vertically upward at atmospheric pressure, and a 35 mm diameter uncooled honeycomb burner at atmospheric pressure. As noted earlier, both burner flows were placed in coflow in order to eliminate oscillations associated with burner stabilized flames at atmospheric pressure. As noted earlier, both burner flows were placed in coflow in order to eliminate oscillations associated with burner stabilized flames at atmospheric pressure. Room disturbances were controlled by surrounding the flames with layers of screens and a plastic enclosure. The combustion products were removed using the laboratory exhaust system. The burner assemblies could be traversed in the horizontal and vertical directions in order to accommodate rigidly mounted optical instrumentation.

Table 2. Summary of Experimental Methods

Measurement	Method
Soot volume fraction	Laser extinction[a]
Soot structure	Transmission electron microscopy[b]
Soot temperature	Multiline emission[a]
Gas temperature	Extrapolated thermocouples[c]
Gas composition	Gas chromatography
Radical (H,O,OH) composition	Li/LiOH atomic absorption[a]
Flow velocities	Laser velocimetry

[a]Deconvoluting measurements for chord-like paths.

[b]Also high resolution transmission electron microscopy (HRTEM).

[c]Extrapolating results for thermocouples having different bead sizes to an infinitely-small bead size.

Table 3. Premixed Flame Test Conditions[a]

Flame	Fuel-Equivalence Ratio	C/O Ratio[b]	F/O Ratio[c]
Ethylene/air flames similar to Harris and Weiner (1983a,b; 1984a,b), from Xu et al. (1997):			
1	2.34	0.78	---
2	2.49	0.83	---
3	2.64	0.88	---
4	2.79	0.93	---
5	2.94	0.98	---
Methane oxygen flames similar to Ramer et al. (1986), from Xu et al. (1998):			
6	2.35	---	1.10
7	2.45	---	1.15
8	2.56	---	1.20
9	2.67	---	1.25
10	2.77	---	1.35

[a]Premixed, 60 mm diameter McKenna Products, Inc. water-cooled flat flame burner directed vertically upward at atmospheric pressure with 6 mm wide annular nitrogen coflow.
[b]Atomic carbon/oxygen (C/O) ratios.
[c]Molar fuel/oxygen flow rate (F/O) ratios.

Table 4. Nonpremixed Flame Test Conditions[a]

Flame	Fuel[b]	Percent Fuel in N_2[c]	Flame Length (mm)
Acetylene-nitrogen/air flames, from Xu and Faeth (2001):			
1	C_2H_2	16.9	82
2	C_2H_2	15.1	80
3	C_2H_2	17.1	103
Hydrocarbon-nitrogen/air flames, from El-Leathy et al. (2001):			
4	C_2H_4	100.0	100
5	C_3H_6	18.8	100
6	C_3H_8	100.0	100
7	$C_6H_6(4\%)/C_2H_2$	85.4	90
8	$C_6H_6(11\%)/C_2H_2$	88.5	90
9	$C_6H_6(29\%)/C_2H_2$	92.3	90

[a]Nonpremixed, 34.8 mm diameter fuel port flowing fuel/nitrogen mixtures vertically upward in coflowing air at atmospheric pressure.
[b]Concentrations are percent by volume in the fuel mixture.
[c]Concentrations are percent by volume in the fuel/nitrogen mixture.

Measurements of flame structure and soot properties were carried out along the axes of the test flames. The measurements that were made and the methods that were used are summarized in Table 2. The laser extinction measurements of soot volume fractions, the

multiline emission measurements of soot temperatures and the Li/LiOH atomic absorption measurements of radical concentrations were all deconvoluted to find radial distributions of the properties in question but only the centerline value was used during present work.

Test conditions for the premixed flame measurements are summarized in Table 3. The test flames included five fuel-rich laminar premixed ethylene/air flames, similar to the flames considered by Harris and Weiner (1983a,b,1984a,b), and five fuel-rich laminar premixed methane-oxygen flames, similar to the flames considered by Ramer et al. (1986).

Diffusion Flame Apparatus. A single burner operating at atmospheric pressure was used for all the diffusion flame measurements. The burner consisted of a 34.8 mm diameter fuel port directed vertically upward, terminated with a honeycomb, and having a 60 mm diameter coannular air port for an air coflow in order to eliminate flow oscillations. The burner was not cooled because the flames were somewhat separated from the burner. Room disturbances were controlled by surrounding the flames with layers of screens and a plastic enclosure. The combustion products were removed using the laboratory exhaust system. The burners could be traversed in the horizontal and vertical directions in order to accommodate rigidly-mounted optical instrumentation. Experimental methods used for measurements in the diffusion flames were the same as in the premixed flames as discussed in connection with Table 2.

Test conditions for the diffusion flame measurements are summarized in Table 4. The experiments began with the acetylene/air flames considered by Xu and Faeth (2001) because acetylene is a basic building block of soot growth via the classical HACA soot growth mechanism (Frenklach and Wang 1990,1994; Colket and Hall, 1994). The fuel was diluted with nitrogen for these tests in order to control maximum soot concentrations in the flames so that excessive buildup of soot on instrumentation probes was avoided. Effects of fuel type were then considered by El-Leathy et al. (2001). The fuel type experiment considered ethylene, propylene and propane as fuels, as well as acetylene/benzene mixtures, again using nitrogen dilution to control soot levels in the flames. In particular, the acetylene/benzene mixtures were used in order to promote the PAH mechanism of soot growth in comparison to the HACA mechanism, because the PAH mechanism is advocated as the main mechanism for soot growth, compared to the HACA soot growth mechanism, by some workers in the field (Bockhorn et al. 1982,1984; Colket and Hall, 1994; Frenklach and Wang 1990,1994; Maus et al., 1994; Kazakov et al. 1995).

2.3 Computational Results

Predictions of flame properties were undertaken for the laminar premixed flames based on the chemical mechanisms of Frenklach and coworkers (1990,1994,1995) and Leung and

coworkers (1991,1995), see Xu et al. (1997,1998) for more details about the mechanisms. The predictions were obtained using the steady one-dimensional premixed flame computer code, PREMIX, of Kee et al. (1985,1986). PREMIX considers mixture-averaged multicomponent diffusion, thermal diffusion, and variable thermophysical and transport properties. Effective of radiative heat losses were handled by using present measurements to prescribe temperature and velocity distributions as functions of distance from the burner.

2.4 Experimental and Computational Results

Soot Structure. A typical TEM photograph of a soot particle (soot aggregate) collected from the present flames is illustrated in Fig. 2. This soot aggregate was obtained during a space-based experiment with a nonbuoyant soot emitting ethylene-fueled laminar jet diffusion flame in still air at 100 kPa; thus, this soot aggregate is generically typical but is somewhat larger than soot aggregates found in buoyant laminar jet diffusion flames having much shorter residence times. The present soot aggregates consist of nearly monodisperse (at a particular flame condition) spherical primary soot particles that generally have diameters smaller than 60 nm. These primary particles collect into soot aggregates of particles that have rather broad ranges of numbers of primary particles per aggregate (typically having 2-2000 primary particles per aggregates). These aggregates are mass fractal objects having fractal dimensions of roughly 1.8 whose optical properties are reasonably represented using the Rayleigh-Debye-Gans scattering approximation with optical models for these particles generally called Rayleigh-Debye-Gans/polydisperse-fractal-aggregate (RDG/PFA) theory, see Köylü and Faeth (1992,1994a,b,1996) for more details about the optical and radiative properties of soot aggregates.

Premixed Flame Structure. Measurements of temperature, velocities, soot volume fractions, primary soot particle diameters, and the concentrations of major gas species along the axis of a methane/oxygen flame having F/O = 1.20 are plotted as a function of height above the burner exit in Fig. 3. Corresponding residence times found by integrating the velocity measurements are shown at the top of the plots; these times are relative to the first position where finite soot volume fractions were measured. These results are qualitatively similar to the structure of other soot-containing premixed flames that were studied, see Xu et al. (1997,1998) for other examples.

Due to relatively small gas velocities at the burner exit (roughly 60 mm/s), and the small densities of the combustion gases, effects of buoyancy are significant and streamwise velocities increase to values greater than 1 m/s at z = 25 mm. Temperatures near the burner exit (before the maximum temperature condition) were in the relatively soot-free region and were measured with

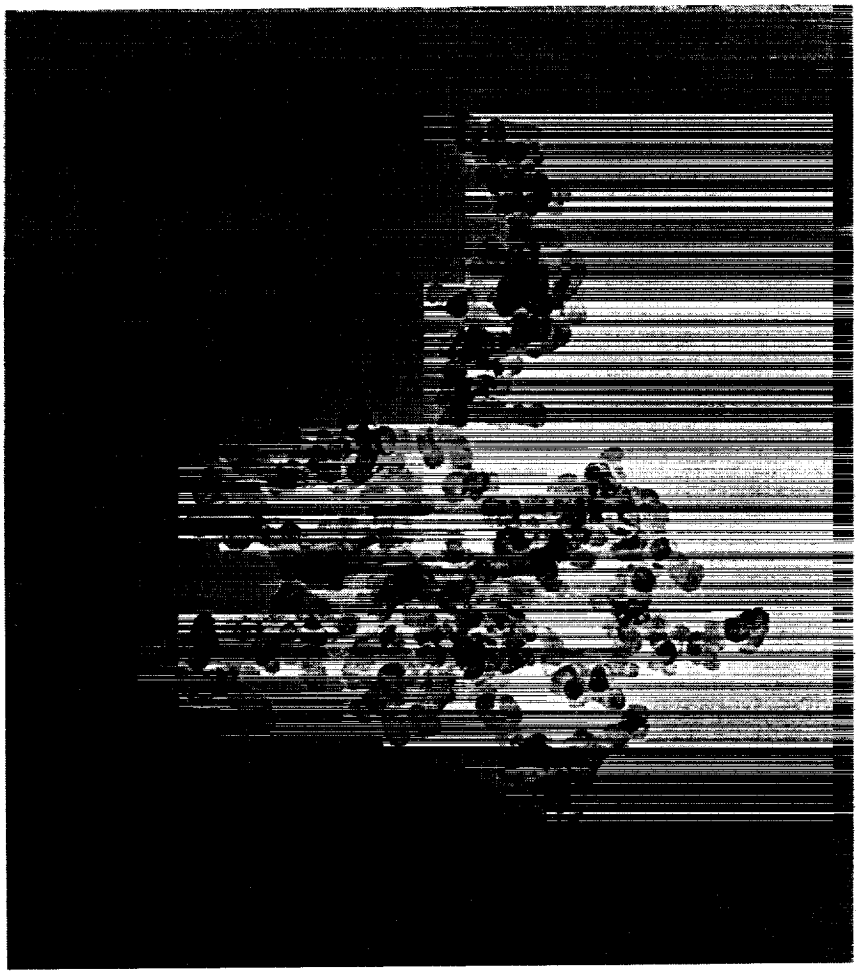

Fig. 2 TEM photograph of a typical soot aggregate in a nonbuoyant round ethylene-fueled laminar jet diffusion flame in still air at 100 kPa. This aggregate was in the soot layer beyond the flame tip (z = 55 mm) of a soot emitting flame. It has a maximum dimension of 1100 nm. From Urban et al. (1998).

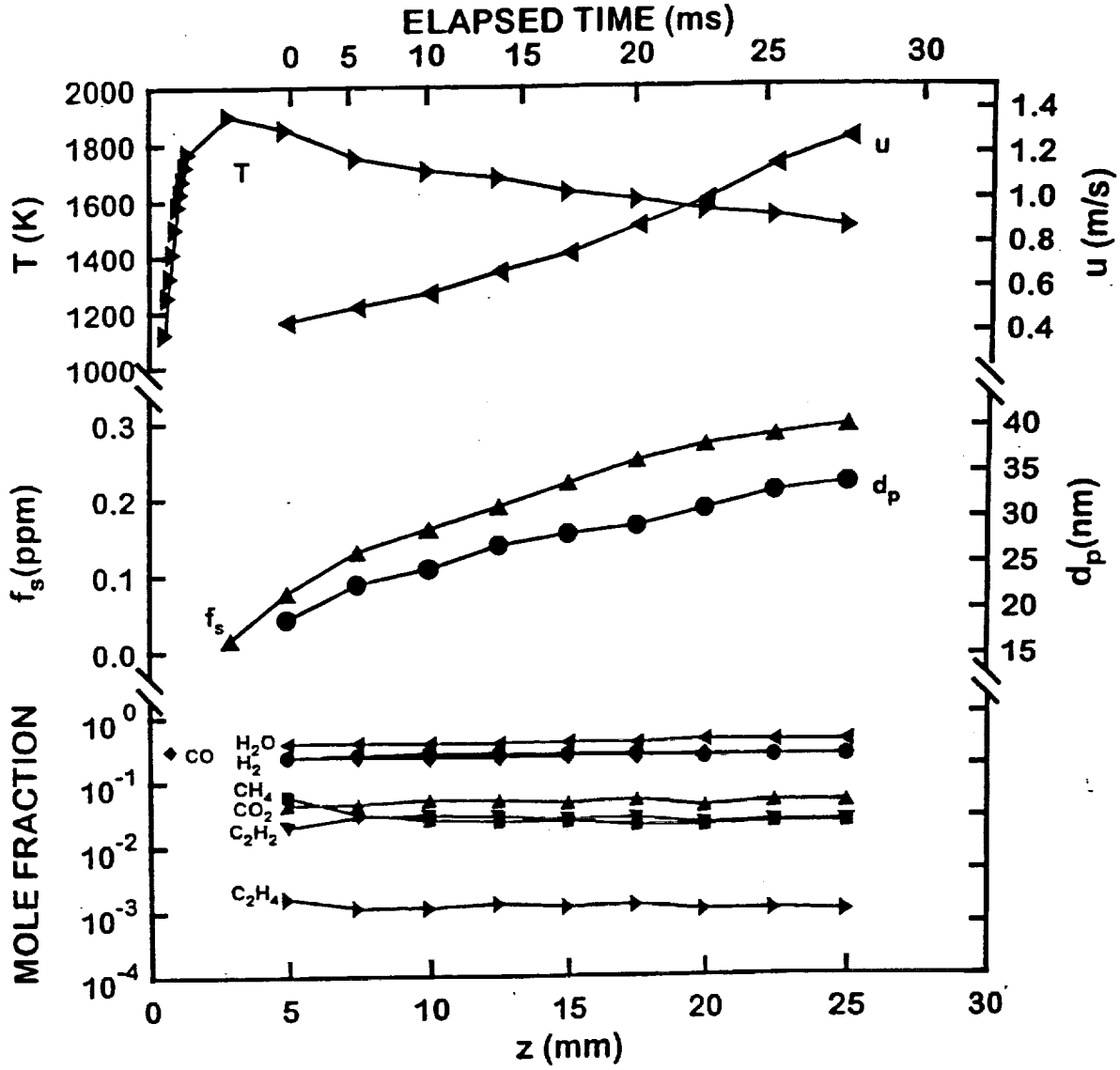

Fig. 3 Measured soot and flame properties along the axis of a laminar premixed methane/oxygen flame with F/O = 1.25 at atmospheric pressure. From Xu et al. (1998).

thermocouples, the remaining temperatures were measured using multiline emission. These flames have significant radiant heat losses due to continuum radiation from soot.

Finite soot volume fractions are first observed 2-3 mm above the burner surface. Soot volume fractions subsequently increase but level off at the highest position shown; as discussed later, this behavior is caused by reduced H concentrations due to reduced temperatures because soot growth and nucleation rates are both quite dependent on H concentrations (the former through the HACA soot growth mechanism). Primary particle diameters generally could be measured at conditions where soot volume fractions could be measured with reasonable accuracy; such conditions involved primary particle diameters larger than 15 nm.

Concentrations of major gas species are nearly constant and are little affected by soot formation (which involves less than 0.02% of the mass of carbon in the reactants). Hydrocarbons having the largest concentrations are methane, acetylene and ethylene with acetylene thought to be the major producer of soot through the HACA mechanism.

The measured yields of major gas species for the various methane/oxygen flames are plotted in Fig. 4 along with predictions using the chemical mechanisms of Leung and Lindstedt (1995) and Frenklach and Wang (1990). The measurements also include results of Ramer et al. (1986) for the same flames. These results are for a position located 20 mm above the burner exit but the results illustrated in Fig. 3 suggest that concentrations of major gas species are relatively independent of streamwise distance. Present measurements are in good agreement with the earlier measurements of Ramer et al. (1986) and the predictions based on the chemical mechanisms of Leung and Lindstedt (1995) and Frenklach and Wang (1990) also are in excellent agreement with each other and with the measurements. The largest discrepancies between the measurements and the predictions are that predictions generally underestimate measured CH_4 concentrations at small F/O ratios and somewhat overestimate C_2H_2 concentrations at large F/O ratios. Discrepancies between measurements and predictions for premixed ethylene/air flames were similar (Xu et al., 1997).

Measured and predicted H concentrations in the soot formation region of laminar methane/oxygen premixed flames having fuel equivalence ratios of 2.45, 2.56 and 2.67 are plotted as a function of height above the burner exit in Fig. 5. Similar to earlier predictions of major gas species in Fig. 4, the predictions of H concentrations using the mechanisms of Leung and Lindstedt (1995) and Frenklach and Wang (1990) are essentially the same and similar to results found in laminar premixed ethylene/air flames (Xu et al., 1997). Furthermore, the model predictions are in excellent agreement with estimates based on the assumption of local thermodynamic equilibrium of H concentrations. Finally, the agreement between the various

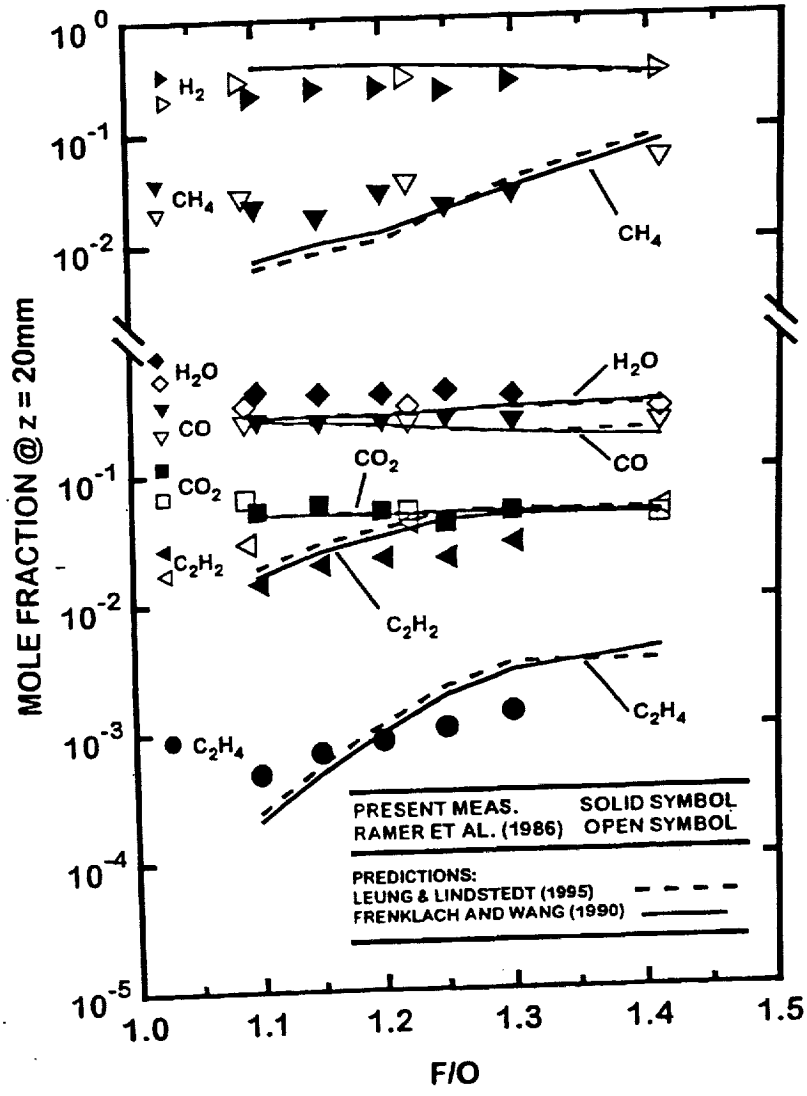

Fig. 4 Measured and predicted concentrations of major gas species at the axis of laminar premixed methane/oxygen flames at z = 20 mm and atmospheric pressure. From Xu et al. (1998).

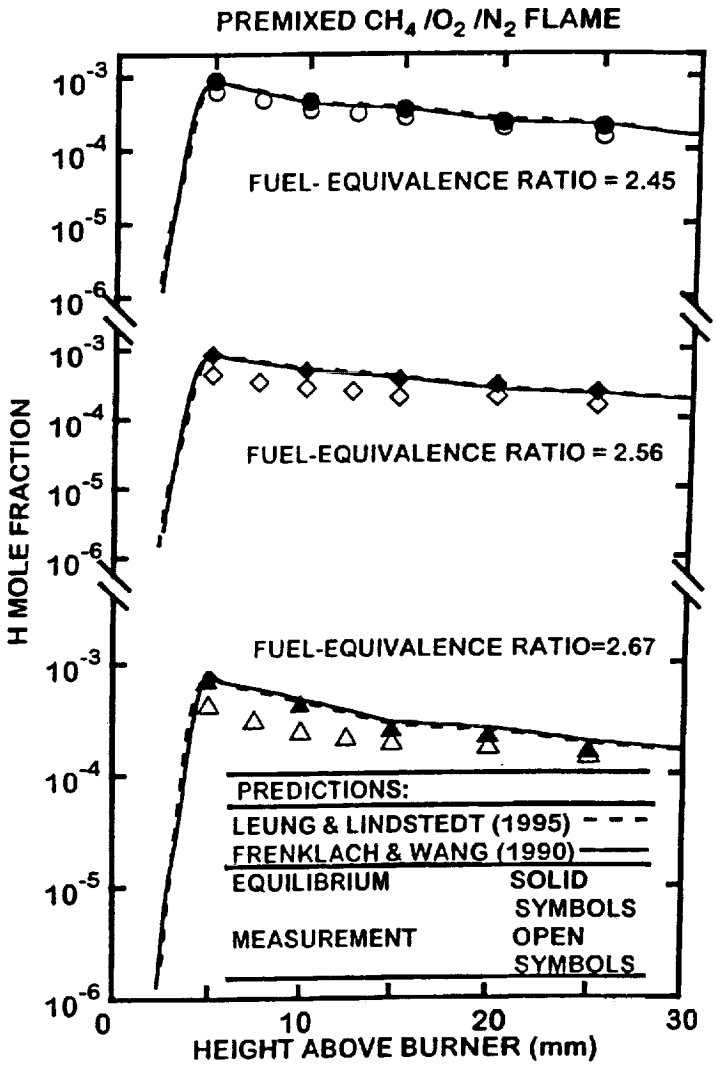

Fig. 5 Measured and predicted H concentrations along the axes of laminar premixed methane/oxygen flames at atmospheric pressure. From Xu and Faeth (2000).

predictions and the measurements is also excellent. Such behavior, however, is quite reasonable due to the relatively slow evolution of properties within the soot growth region. Based on these observations, the reductions of H concentrations with increasing streamwise distance can be attributed to reduced flow temperatures caused by radiative heat losses (largely due to continuum radiation from soot itself). Subsequently, reduced H concentrations cause reduced growth rates leading to the end of soot formation in premixed flames, as seen in Fig. 4, through the HACA soot growth mechanism (this will be shown more definitively, subsequently). Thus, there is no need to invoke processes of soot aging, proposed by early workers in the field, to explain the end of soot growth in premixed flames.

Diffusion Flame Structure. Typical measurements of gas (soot) temperatures, streamwise gas velocities, soot volume fractions, primary soot particle diameters, the concentrations of major gas species and the concentrations of radical (H, OH, O) species are plotted as a function of height above the burner exit for an acetylene-nitrogen-fueled laminar jet diffusion flame burning in coflowing air in Fig. 6. These results are for an atmospheric pressure flame from Xu and Faeth (2001). Corresponding residence times, found by integrating the velocity measurements, are shown at the top of the plot; these times are relative to the first position when detectable soot volume fractions were observed (roughly z = 10 mm). Composition measurements for this flame show that all the measurements in Fig. 6 were made at fuel-rich conditions (with fuel equivalence ratios greater than 1.10). Gas (soot) temperatures reach a maximum well before regions of greatest soot production in Fig. 6 and the flame sheet (where $\phi = 1$) and maximum temperatures are smaller than stoichiometric temperatures for these flames. These trends are similar to earlier observations of Sunderland et al. (1995) for acetylene-nitrogen-fueled laminar coflowing jet diffusion flames burning in air at subatmospheric pressures. This behavior is mainly caused by significant effects of continuum radiation from soot, with potential contributing effects of preferential diffusion of species and heat.

Primary soot particle diameters reach a maximum early in the soot formation region, which is caused by accelerating nucleation rates with increasing streamwise distance (Xu and Faeth (2001). Significant levels of soot formation begins at conditions where detectable concentrations of H are first observed and end where concentrations of acetylene become small. The soot formation region, however, contains significant concentrations of species associated with soot oxidation, e.g., OH, O_2 and O, so that soot formation and oxidation proceed at the same time.

Concentrations of major gas species seen in Fig. 6 are in general agreement with the earlier observations of Sunderland et al. (1995). Acetylene and O_2 concentrations decrease and increase monotonically throughout the soot formation region, whereas the intermediate

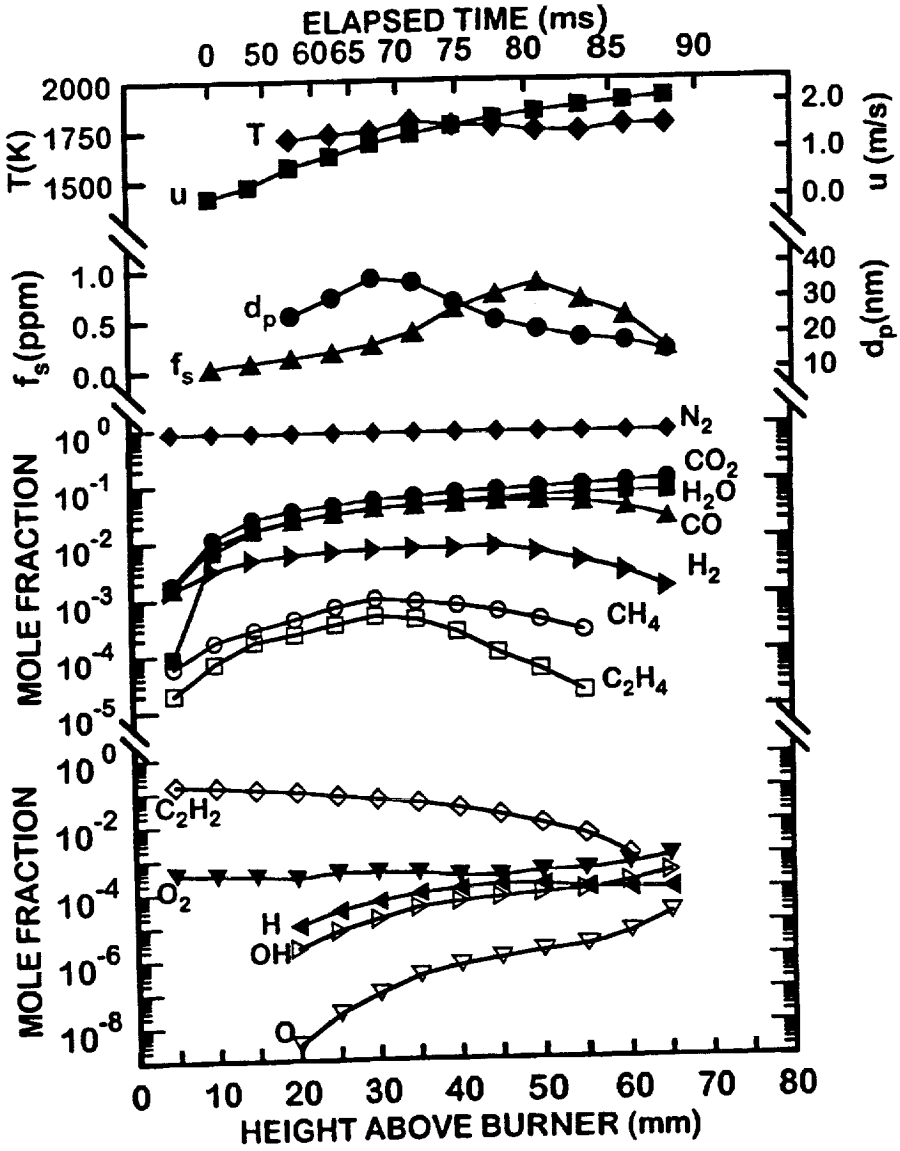

Fig. 6 Measured soot and flame properties along the axis of an acetylene-nitrogen/air laminar jet diffusion flame at atmospheric pressure (16.9% acetylene by volume burner flow). From Xu and Faeth (2001).

hydrocarbons CH_4 and C_2H_4 reach maxima when primary particle diameters reach a maximum. In addition, H_2 and CO, associated with water-gas equilibrium, are present in large concentrations at soot formation conditions. Finally, concentrations of the radials, H, OH and O progressively increase as the flame sheet, where they mainly are produced, is approached.

The measured H, OH and O concentrations in the acetylene-nitrogen/air laminar jet diffusion flames at atmospheric pressure are illustrated in Fig. 7. These measurements are compared with equilibrium estimates of radical concentrations and presented as superequilibrium ratios in the figure. The results show that H, OH and O approach equilibrium concentrations near the onset of soot formation but eventually reach superequilibrium ratios in excess of 10-20 as the flame sheet is approached. The fact that H concentrations approach equilibrium in premixed flames but generally are present in superequilibrium concentrations in diffusion flames accounts for the larger rates of soot formation in diffusion flames than in premixed flames having comparable acetylene concentrations and temperatures, through the HACA mechanism (Sunderland et al., 1997).

The structure of an ethylene-fueled laminar jet diffusion flame in coflowing air at atmospheric pressure is illustrated in Fig. 8. This plot is essentially in the same format as Fig. 6 for acetylene-nitrogen-fueled flames. It is evident that the soot formation region in Fig. 8 is dominated by large concentrations of acetylene, very similar to the acetylene-fueled flame illustrated in Fig. 6. Thus, the fuel mainly decomposes to yield large concentrations of acetylene and H which subsequently reacts to form soot through the HACA mechanism. This proved to be the case for all the hydrocarbon fuels considered in Table 3 for premixed flames and considered in Table 4 for diffusion flames. Thus, even in the case of an aromatic fuels such as benzene, present observations did not provide evidence of soot growth paths (e.g., a PAH path) alternative to the HACA mechanism.

2.5 Conclusions

Flame and soot structure properties were studied in the ethylene/air and methane/oxygen laminar premixed flames summarized in Table 3 and in the hydrocarbon/air laminar jet diffusion flames summarized in Table 4, all of which were at atmospheric pressure. Major conclusions drawn from the observations of the premixed flames are as follows:

1. Predictions of the yields of major gas species using PREMIX and the mechanisms of Leung and Lindstedt (1995) and Frenklach and Wang (1990) were in good agreement with each other, and with present measurements, which is very encouraging because present flames involved potential complications due to the presence of soot.

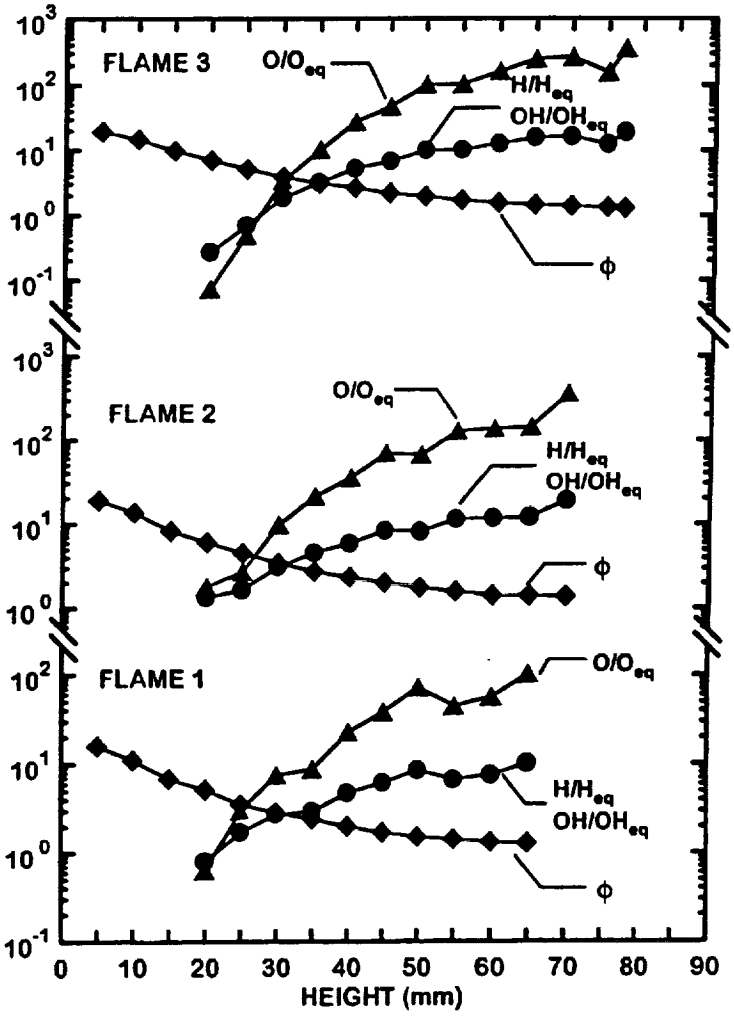

Fig. 7 Radical species concentrations in acetylene/air laminar jet diffusion flames at atmospheric pressure. Measurements from Xu and Faeth (2001).

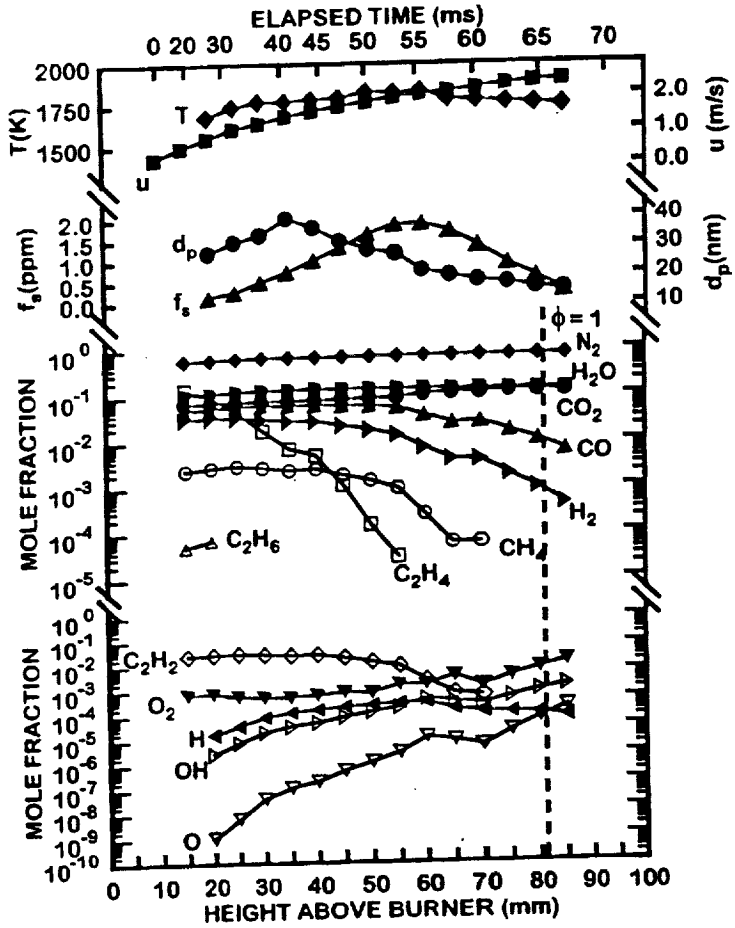

Fig. 8 Measured soot and flame properties along the axis of an ethylene-nitrogen/air laminar jet diffusion flame at atmospheric pressure (100.0% ethylene by volume burner flow). From El-Leathy et al. (2001).

2. H-atom concentrations generally satisfy the requirements of local thermodynamic equilibrium within the soot growth region of laminar premixed flames (which is well downstream of the main reaction zone). This observation is justified by both measurements and predictions of flame structure and is perhaps not surprising due to the relatively slow evolution of the properties of the soot growth region.

3. Even though yields of H concentrations approximate local thermodynamic equilibrium, the yields of major gas species clearly are not in local thermodynamic equilibrium, e.g., the concentrations of these species typically depart from equilibrium requirements by factors greater than 3.

Corresponding major conclusions drawn from the observations of the diffusion flames are as follows:

1. Measurements show that H, OH and O approach equilibrium near the start of the soot formation region but generally exhibit superequilibrium concentrations (by factors in excess of 10-20) throughout the soot formation region.

2. Measurements show that soot formation in the diffusion flames studied during this investigation generally involves the decomposition of the original fuel to form relatively robust substances such as C_2H_2, CH_4, H_2 and the radicals H, OH and O. Subsequently, soot formation mainly involves the reaction of acetylene and H through the HACA mechanism (which will be demonstrated subsequently). This behavior was observed even when an aromatic compound, e.g., benzene that might be thought to emphasize soot formation paths involving PAH, was present.

3. Measurements showed that significant degrees of net soot formation begins when H first appears and ends when acetylene concentrations become small, highlighting the importance of H and acetylene for the formation of soot in diffusion flames.

(3) / cw / IN / 25

3. Soot Reaction Properties (Ground-Based Study)

3.1 Introduction

Three major soot reaction processes are needed to predict soot properties in flame environments: soot growth, or the formation of soot on soot nuclei and soot particles; soot oxidation, or the reaction of soot with oxidizing species to yield the combustion products of soot